J Nanopart Res (2023) 25:40
https://doi.org/10.1007/s11051-023-05688-4

RESEARCH PAPER

Dissolution control and stability improvement of silica nanoparticles in aqueous media

Laura Spitzmüller · Fabian Nitschke · Bastian Rudolph · Jonathan Berson · Thomas Schimmel · Thomas Kohl

Received: 24 August 2022 / Accepted: 8 February 2023

Abstract Silica nanoparticles have become an important tool in material sciences, nanomedicine, biotechnology, and pharmaceutics, with recent suggested applications also in environmental sciences. In life and environmental sciences, the application field is usually aqueous media; however, the crucial issue of silica nanoparticle dissolution behavior and rate in the target medium is often neglected, overlooked, or taken for granted. Silica nanoparticles are not stable in aqueous solutions until equilibrium silica concentrations are reached. While for life science applications, the degradability of silica nanoparticles is prerequisite for biocompatibility, this characteristic impedes the successful application of silica nanoparticles as environmental tracer, where long-term stability is needed. In this study, the impact of external (temperature, pH values, salinity, availability of silica) and internal (degree of condensation, size, porosity) parameters on the stability of ~ 45-nm-sized silica nanoparticles is characterized. Results show that external factors such as elevated temperature and alkaline pH-values accelerate the dissolution, acidic pH, high salinities, and high initial silica concentrations exhibit a contrary effect. Consequently, in applications, where external parameters cannot be controlled (e.g., in vivo, subsurface reservoirs), dissolution control and stability improvement of silica nanoparticles can be achieved by various means, such as adding a protective layer or by condensation of the silanol bonds through calcination.

Keywords Nanotracer · Drug carriers · Silica nanoparticles · Degradation · Surface modifications · Geothermal · Environmental effects

Supplementary information The online version contains supplementary material available at https://doi.org/10.1007/s11051-023-05688-4.

L. Spitzmüller (✉) · F. Nitschke · B. Rudolph · T. Kohl
Institute of Applied Geosciences, Division of Geothermal Energy & Reservoir Technology, Karlsruhe Institute of Technology, Adenauerring 20b, 76131 Karlsruhe, Germany
e-mail: laura.spitzmueller@kit.edu

L. Spitzmüller · B. Rudolph · J. Berson · T. Schimmel
Institute of Nanotechnology, Karlsruhe Institute of Technology, Hermann-von-Helmholtz-Platz 1, 76344 Eggenstein-Leopoldshafen, Germany

L. Spitzmüller · B. Rudolph · J. Berson · T. Schimmel
Institute of Applied Physics, Karlsruhe Institute of Technology, Wolfgang-Gaede-Straße 1, 76131 Karlsruhe, Germany

Introduction

Over the last decades, silica nanoparticles gained worldwide importance and attention [1]. The well-established industrial applications, e.g., application in material sciences, have in common that the silica nanoparticles are applied in/to dry environments, where silica nanoparticles are considered inert and

Published online: 18 February 2023

stable [2]. Over the last decade, engineered silica nanoparticles have been developed for biomedical purposes, e.g., serving as tunable nanocarriers for water-insoluble drugs, chemotherapeutics, and as soluble drug encapsulation facilitating long-term release applications [3–14]. The favorable properties of silica nanoparticles were furthermore highlighted by the easily functionable surface, e.g., for targeted or stimuli-responsive drug release [10, 13, 15–17], and in the field of nanobiophotonics [4, 18–22]. Additionally, the small size of the nanoparticles offers the unique opportunity of reaching formerly inaccessible areas, e.g., across the blood–brain barrier [3, 22, 23]. The usage of nanoparticles as imaging sensors in life sciences inspired research toward similar applications in the environmental sciences. In particular, hydrology and geothermal production are often facing the challenge of an exploitation from inaccessible reservoirs. However, a sustainable management of a reservoir and the long-term optimized commercial production requires a comprehensive knowledge about the structures and flow paths and their hydraulic behavior. For such analysis, well-established tracing techniques usually use fluorescent molecular dyes such as sodium fluorescein or eosin [24]. However, molecular dyes can be greatly affected by fluids pH and temperature and have a low photostability [25–27]. In addition, the rock properties of the underground can lead to adsorption and in extreme cases to complete retention of molecular tracers and impede the characterization of the reservoir. Thus, there is the requirement for new approaches to overcome the drawbacks of the molecular dyes. Basic research has been conducted on the application of silica nanoparticles as tracers in hydrology for aquifer and reservoir assessment [28–33]. Further developments led to advanced temperature-sensitive silica nanoparticles as tracers for geothermal reservoir characterization [33–35].

For all application in aqueous environments (geothermal tracer, groundwater marker, bioimaging, drug delivery, theranostic), the stability of the silica nanoparticles is a key parameter. Two factors are therefore of utmost importance: the silica solubility (i.e., the maximum SiO_2 concentration to attain equilibrium at given geochemical conditions) and the silica dissolution rate. From the environmental sciences, it is well known that the stability of silica, silicates, and other SiO_2-polymorphs depends mainly on the crystallinity of the silica network, with higher crystalline order being less soluble [36]. The dissolution process of silica in water can be described in simplified form:

$$SiO_2 + 2H_2O \rightleftharpoons H_4SiO_4 \quad (1)$$

with H_4SiO_4 the monomeric, silicic acid species. This reaction takes place until the equilibrium, the thermodynamically governed silica saturation concentration (SSC), is reached. From natural systems, it is also well-known that elevated temperatures augment the SSC and increase the silica dissolution kinetic [37–39]. Studies found the SiO_2 concentration at equilibrium with amorphous silica, referred to as silica saturation concentration (SSC), to be in the range of 90 mg L^{-1} to 170 mg L^{-1} at room temperature and increasing up to the range of 270 mg L^{-1} to 310 mg L^{-1} at 80 °C [39–43]. The broad variation can be explained by differences of the natural amorphous silica itself such as the degree of hydration, the presence of areas of higher degree of crystallinity, the amount of impurities, and the particle size [36]. However, in fact, the proportionality of silica concentration in natural groundwater and geothermal fluids and their temperature is a widely used tool to deduce the subsurface temperature from the composition of natural springs [39, 44–46]. Temperature is therefore expected to have also a high impact on the dissolution of artificial silica nanoparticles. Other important factors that are affecting the solubility of natural silica are pH and salinity of the solution. Hence, they are assumed to affect the solubility of artificial silica nanoparticles as well.

Even though artificial silica nanoparticles are mainly of an amorphous structure, differences in the degree of condensation of the silica network deriving from the synthesis makes comparison with natural amorphous silica not expedient. In particular, tunable properties like size, shape, porosity, functionalization, and the high surface area of the silica nanoparticles complicate the analysis of behavior of silica nanoparticles in aqueous environments. Thus, only sparse data on the (aqueous) stability of artificial silica nanoparticles exist [47]. Additionally, although several studies on the safety of silica nanoparticles in biological media or in vivo [48–60] and ecotoxicological assessments [61, 62] exist, the data situation is complex and partly contradicting, as there is no standardized testing procedure. The main consent seems to be the dependency on many factors, e.g., on dosage, cell

type, protein corona, surface functionalization, size, and shape the particles [20, 49, 51, 54, 63–66], and the nontoxicity and biocompatibility of the degradation product silicic acid [23, 67]. Therefore, the degradability of silica nanoparticles is a desired factor for most applications in life science. However, for long-term drug release, a slow, controlled, and well-characterized drug release would be beneficial, as degradation of the carrier's matrix would lead to premature release of the incorporated drugs [68]. Furthermore, the degradability of silica nanoparticles is up to now the major obstacle for hydrology and geothermal applications, where high (thermal) and long-term stability is crucial. Therefore, accurate knowledge of the degradation process by identifying factors affecting the dissolution rate and the solubility of silica is of utmost importance for both, life and environmental science applications [69–71]. No fundamental studies have been performed on the individual effect of temperature, salinity, pH, particle concentration, and initial silica concentration on the stability of artificial silica nanoparticles. This study aims to bridge the gap and obtain detailed knowledge of the behavior of artificial silica nanoparticles in aqueous environments by first performing a sensitivity study on the impact of various parameters on the stability of silica nanoparticles in aqueous media and second, the development and evaluation of surface modifications strategies for silica nanoparticles stability enhancement. For this study, nonporous, fluorescent ~ 45 nm silica nanoparticles were chosen to represent a possible tracer for environmental sciences [35] and simultaneously represent a possible usage in bioimaging [72]. Especially for the application in environmental sciences, the fluorescence is beneficial for monitoring of tracer breakthrough and return curves. Within this study, we examine the individual effects of temperatures up to 80 °C, pH values ranging from pH 3 to pH 11, salinity of mono- and divalent ions up to concentrations of 4 mol L^{-1}, physiological buffer solution PBS (phosphate-buffered saline) at 37 °C, silica nanoparticle concentrations up to 1 mg mL^{-1}, and initial silica concentrations up to 250 mg L^{-1} on the stability of non-porous silica nanoparticles in aqueous solution over an application-relevant period of time and characterize the dissolution kinetics. Additionally, the stability of selected mesoporous silica particles was tested under physiological/biomedical relevant conditions. Finally, although several approaches exist modifying the surface of silica nanoparticles; either by adding a protective layer on the surface, organic functionalization or even by calcination of the particles [64, 67, 73–77], their impact on the SSC and dissolution kinetic is yet not monitored sufficiently. We therefore tested and compared several approaches; chemical surface modifications including silanization (octadecyltrimethoxysilane and 1,2-Bis(trimethoxysilyl)decane), grafting of paraffin (dotriacontane) and metal oxide coating, as well as calcination (300 °C, 500 °C, and 700 °C).

Materials and methods

Synthesis

Reversed microemulsion (fluorescent nanoparticles)

The particle synthesis starts with a mixture of cyclohexane (VWR Chemicals AnalaR Normapur, 15 mL), *n*-Hexanol (VWR GPR Rectapur, Assay < 98%, 3.6 mL) and Triton X 100 (Sigma-Aldrich for analysis, 3.44 mL) magnetically stirred in a round bottom flask. After 1 min reaction time, Tris(2,2-bipyridyl)dichlororuthenium(II) hexahydrate ($Ru(bpy)_3^{2+}$, Acros organics, 98%, 0.96 mL 20 mM) and tetraethylorthosilicate (TEOS, Sigma-Aldrich, 99.0%, 0.2 mL) are added. After 20 min of continued stirring, ammonium hydroxide solution (Merck, 28–30%, 0.12 mL) is added. After 24 h continued stirring, acetone (VWR Chemicals AnalaR Normapur, 28 mL) is added to break down the microemulsion. The solution is then collected, centrifuged at 4400 g (6000 rpm, Hermle Z206A) and undergoes 4 washing-centrifugation cycles using acetone, ethanol, ethanol + water (80:20), and water. A 5th cycle (ethanol) can be added optionally to facilitate vacuum drying of the particles. When needed, a sonotrode (IUP200St, Hielscher Ultrasonics) or a sonication bath (Bandelin Sonorex) was applied to resuspend the pellets. The fluorescent particles show sizes of 44 ± 3 nm and an average ζ-potential of − 37.2 ± 2.3 mV.

Stöber synthesis (non-fluorescent nanoparticles)

Stöber synthesis following Stöber et al. [78]. Ethanol (26 mL) were mixed with H_2O (1.6 mL) and ammonium hydroxide (3 mL). After thoroughly stirring,

tetraethylorthosilicate (3 mL) is added and the solution is stirred for 2 h at 60 °C. The solution is then collected and centrifuged at 4400 g (6000 rpm) and undergoes 3 washing cycles with ethanol and water.

Surface modifications

1,2-Bis(Trimethoxysilyl)decane

The coating of the fluorescent nanoparticles with 1,2-Bis(trimethoxysilyl)decane (Gelest Inc.) was performed following the procedure of Arkles et al. [79]. Acetonitrile (Merck, 99.5%) was used as solvent. 1,2-Bis(trimethoxysilyl)decane (1 wt%) was added to the solution and stirred for at least 20 h. The nanoparticles are collected via centrifugation and dried in vacuum.

Octadecyltrimethoxysilane

Starting from the fluorescent nanoparticle synthesis, the NPs are dried and weighted. Dry acetonitrile (Merck, 99.5%) and *n*-Octadecyltrimethoxysilane (ABCR GmbH, 95%, 0.375 mL) per 50 mg particles is added. After stirring the solution for at least 12 h, the nanoparticles are collected by centrifugation. One washing cycle with acetonitrile and one with hexane (Carl Roth, 99%) is performed. Then the particles are dried in vacuum. No surfactants were used to resuspend the particles in water for the stability experiments.

Dotriacontane

Starting from the capping with *n*-Octadecyltrimethoxysilane, the dried particles are resuspended in hexane (40 mL) per 50 mg particles and dotriacontane (Sigma-Aldrich, 97%, 375 mg) per 50 mg particles are added. The solution is sonicated for 15 min, followed by a 15-min stirring cycle. The particles are collected by centrifugation and dried in vacuum. No surfactants were used to resuspend the particles in water for the stability experiments.

Titania coating

The coating with titania was performed following Joo et al. [80]. Then, 50 mg fluorescent nanoparticles are dispersed in ethanol (20 mL) and stirred at 500 rpm. Hydroxylpropyl cellulose (Acros Organics, 0.1 mg) and H_2O (0.1 mL) were added. Tetrabutyl orthotitanate (1 mL, TBOT, Sigma-Aldrich, synthesis grade) was mixed with ethanol (4 mL) and added with a syringe pump with 0.5 mL min^{-1}. The solution was heated up in an oil bath to 85 °C. After 100 min, the nanoparticles are collected by centrifugation.

Calcination

The calcination of the non-fluorescent nanoparticles was performed using a quartz cuvette and an oven at the temperatures desired. The particles are heated for 24 h and used afterwards as retrieved.

Experimental procedure

For the stability experiments, 1 mg mL^{-1} silica nanoparticle concentration and deionized water (18 MΩ) was used unless otherwise noted. First, the particles were dispersed in the aqueous media using a sonication bath. The experiments were performed under static conditions without disturbance of the dispersions by sonication or stirring. The duration of the experiments is displayed directly in the figures, either as timescale on the *x*-axis, or if sampled at a specific time point, on the *y*-axis. Samples were taken according the following procedure: 50 µL of solution are diluted 1/100 with deionized water. The dissolution experiments were monitored by determination of the amount of dissolved silica in solution. For determination, the silico-molybdenum blue method [36] was performed. After a reaction time of 10 min, the sample was measured with the UV–VIS.

Temperature experiments

Temperature experiments were performed in round glass bottom flasks heated in a silicon oil bath at the desired temperatures. To minimize evaporation, the experiments were performed under reflux. Contamination by dissolution of silica from the glass flasks was excluded as the blank silica concentration did not increase over one week at 80 °C and was negligible.

pH experiments

pH buffer solutions are produced as follows: pH 3 (potassium hydrogen phthalate

[Sigma-Aldrich]—hydrochloric acid [Honeywell Fluka]), pH 4 (potassium hydrogen phthalate—hydrochloric acid), pH 5 (potassium hydrogen phthalate—sodium hydroxide [Merck Emsure]), pH 6 (sodium citrate tribasic dihydrate [Sigma Aldrich]—citric acid [Sigma-Aldrich]) pH 7 (Tris [Carl Roth, ≥ 99.9%]—hydrochloric acid), pH 8 (Tris–hydrochloric acid), pH 9 (glycine [VWR life science, proteomics grade]—sodium hydroxide), pH 10 (glycine—sodium hydroxide), pH 11 (bicarbonate [Sigma-Aldrich]—sodium hydroxide). Experiments were performed at room temperature using centrifuge tubes to avoid silica contamination from glass vessels especially at high pH values.

Salinity experiments

Calcium chloride (VWR technical), sodium chloride (VWR GPR Rectapur), and potassium chloride (VWR GPR Rectapur) were used as purchased. The particles were suspended in the salt solutions. The experiments were performed at room temperature using centrifuge tubes.

Phosphate-buffered saline experiments

For the experiments using a simulated physiological solution, PBS (VWR life science, biotechnology grade) was used. PBS is a buffer solution composed of 137 mM NaCl, 2.7 mM KCl, and 12 mM phosphate. The pH is fixed at 7.4. Different amounts of nanoparticles (nonporous, fluorescent ~ 44 nm), mesoporous nanoparticles (MSN, Sigma-Aldrich Silica mesoporous, 0.5 µm particle size, pore size 2 nm), and mesoporous microparticles (SBA-15, Sigma-Aldrich, Silica mesoporous SBA-15 < 150 µm particle size, pore size 6 nm, hexagonal pore morphology) are added to the PBS solution and heated in a water bath to 37 °C.

Availability of silica experiments

The solutions with variable amount of initial silica were prepared following the procedure of Spitzmüller et al. [81]. Silica (Merck, extra pure) and deionized water were mixed in a HDPE vessel and the pH was adjusted by addition of sodium hydroxide to pH 12. The solution was stirred overnight at 70 °C in an oven. Afterwards, the solution was cooled down to room temperature and the pH was readjusted to pH 7 by addition of hydrochloric acid. The solutions were used immediately after pH adjustment to avoid polymerization and aging especially in oversaturated solutions.

Analytical devices

Spectrophotometric analysis

For the determination of the dissolved silica concentration (mainly Q^0, subordinate Q^1 and Q^2), the molybdenum blue method is used. The Q^0 species reacts with the Silicate (silicic acid) Test from Merck Supelco forming the blue silicomolybdic acid. For measurement of the silica concentration by photometry, an UV–VIS Perkin-Elmer Lambda 9 spectrometer is used ($\lambda = 810$ nm). Samples are diluted using deionized water to assure being in linear range of the Lambert–Beer-Law. Then, 1 mg mL^{-1} SiO_2 standard (Carl Roth) was diluted 1/100 and measured repeatedly as reference for the calibration line. The deviations represent the error of the measurements and are depicted as error bars in the figures in "Results and discussion" section. Reactions of the method with the colloidal species (Q^n) can be excluded as a test series with particles in solution, filtered (0.2 µm acetate filter) and supernatant (centrifugation 6000 rpm/4400 g, 30 min) did not exhibit a significant difference of the silica concentration measured.

SEM

For the SEM images, a Zeiss Leo 1530 was used. The aperture size was set to 30 µm. The EHT was with 1 kV to 2 kV relatively low. These low voltages are necessary due to the sample preparation. The nanoparticles were diluted with ethanol and one drop was put on a p-doted silicon wafer. The wafer was placed on top of an adhesive carbon-tab. With this procedure, the coating with carbon or gold was avoided. However, as the conductivity was low, only low voltages are used to not charge the samples. The working distance was usually around 1.5 to 2.5 mm.

FT-IR-ATR

For the FT-IR-ATR analysis, the Nicolet iS50 was used. The wavenumbers were between 400 and

4000 cm^{-1}. Twenty repetitions were performed. The samples were measured in dry conditions after vacuum drying or calcination.

Results and discussion

For the following experiments, nonporous, fluorescent silica nanoparticles were synthesized using the reversed microemulsion method. Fluorescent particles were chosen to represent the nanoparticles used for most of the environmental applications and for bioimaging, which require such a tracing function. The particles exhibit a spherical shape, with sizes of 44 ± 3 nm and an average ζ-potential of -37.2 ± 2.3 mV. For the stability experiments performed in this study, 1 mg mL^{-1} silica nanoparticle concentration and deionized water (18 MΩ) was used unless otherwise noted. In the course of the experiments, the pH values of the non-buffered solutions ranged between pH 7 and pH 6.2, which is due to the formation of silicic acid. The pH value decreases with increasing amount of dissolved silica. However, this pH range is not expected to additionally affect effectively the dissolution process of silica nanoparticles. For further details to the experimental procedure and the methods used, see the "Materials and methods" section.

Effect of temperature

To monitor the impact of temperature on particle dissolution, the evolution of silica concentration in solution over a 28-h period at 20 °C (room temperature, RT), 40 °C, 60 °C, and 80 °C was measured (Fig. 1). Highlighted in colored areas in Fig. 1 are the silica saturation concentration (SSC) ranges at the respective temperatures derived from literature data and depending on the type of silica [39–43]. SEM-images of the silica nanoparticles after immersion for 24 h at RT and 80 °C (Fig. S 1) show significant particle disintegration and dissolution at elevated temperatures. Since the initial particle concentration was 1 mg mL^{-1} and therefore above the SSC (i.e., c(Si)particles > c(Si)SSC, also defined as excess silica concentration—ESC) for all temperatures, the particles do not need to be completely dissolved to form an equilibrated solution, i.e., to reach the SSC. However, if the amount of silica nanoparticles is too high, all particles would exhibit only minimal dissolution and therefore only minimal size changes. In this case, monitoring the change of the particle size as an indicator of (thermal) stability using DLS or SEM can lead to less reliable results, as the changes may be below detection limit. This might explain the contradicting statements on thermal (in)stability in [32, 33], although the tests of contradicting results were conducted using the exact same silica nanoparticles.

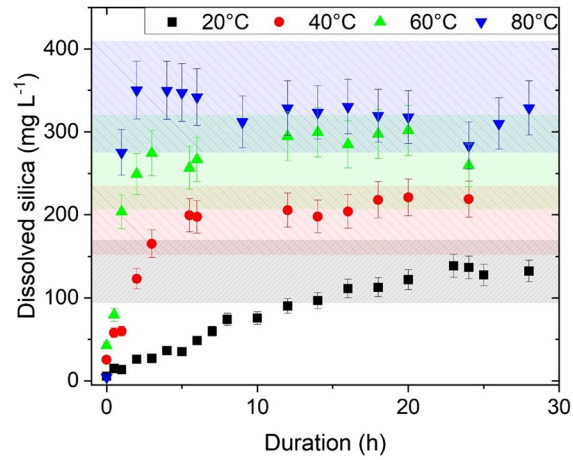

Fig. 1 Time and temperature dependent dissolution of 1 mg mL^{-1} silica nanoparticles in deionized water over a 28-h time period at various temperatures. Highlighted in colored areas the saturation concentration ranges at the respective temperatures (black 20 °C/RT, red 40 °C, green 60 °C, blue 80 °C). Higher temperatures increase both, the silica saturation concentration (SSC) and the dissolution rate. The error bars are determined by the deviations of standard solutions to the calibration line

Kinetic and thermodynamic dissolution

Figure 1 shows furthermore the kinetic and thermodynamic properties of the silica nanoparticle dissolution. Higher temperatures increase both the SSC and the dissolution rate. At RT, the saturation concentration is reached within 28 h, whereas at 80 °C, the dissolution rate increases and the SSC is reached within 2 h (Fig. 1). With the experimental data, the following formula could be established to describe mathematically the dissolution behavior of silica nanoparticles in dependence of temperature:

$$c = SSC * (1 - e^{-kt}) \quad (2)$$

with c the silica concentration in mg L^{-1}, SSC the (thermodynamic) silica saturation concentration in mg L^{-1}, k the (kinetic) temperature-dependent dissolution constant in h^{-1}, and t the time in hours. The relation between temperature and dissolution constant can be determined by a linear regression (Fig. 2b) and can be expressed as:

$$\ln(k) = 2.32 * \ln(T) - 9.58 \tag{3}$$

with T in °C. Equation 3 can be then reformulated to:

$$k = e^{(2.32*\ln(T)-9.58)} \tag{4}$$

The SSC shows a linear temperature dependence up to 80 °C and can be expressed as:

$$SSC = 2.89 * T + 99.62 \tag{5}$$

For predicting the dissolution behavior of silica nanoparticles at a given temperature between 20 and 80 °C in deionized water, Eqs. (4) and (5) are used to determine the temperature-dependent factors k and SSC. Subsequently, the dissolution behavior can be modeled applying Eq. (2). This was done for 20 °C, 40 °C, 60 °C, and 80 °C and the resulting curves are displayed in Fig. 2a (lines) in direct comparison with the experimental data (symbols).

The dissolution rate is further obtained by derivation of Eq. (1):

$$dc/dt = SSC * k * e^{-kt} \tag{6}$$

and depends on the SSC, the dissolution constant k, and the time t. The SSC is a critical value, as it represents the solubility limit of silica and does not only depend on the temperature but also on the crystallinity of the silica nanoparticles, the pH value, and the salinity of the solution. We further expect the dissolution constant k to be dependent on these factors and in addition, on the surface area of the nanoparticles and the initial silica concentration in solution. Figure 2a exhibits the quantification of the kinetics and solubility dependence on temperature by applying Eqs. (2), (4), and (5). The exponential dependence of the dissolution kinetic of the silica nanoparticles is in agreement with kinetic data of amorphous silica obtained by Rimstidt and Barnes [42]. The temperature-dependent formulations of the dissolution behavior found here only serve as an exemplary conduct and are not generally applicable for all types of silica nanoparticles, as the factors SSC and k depend also on other factors such as the particle surface area and need to be individually determined for each case where predictions of silica nanoparticle dissolution are desired. We therefore waive further modeling of the data in this study as it would not lead to a general applicable equation.

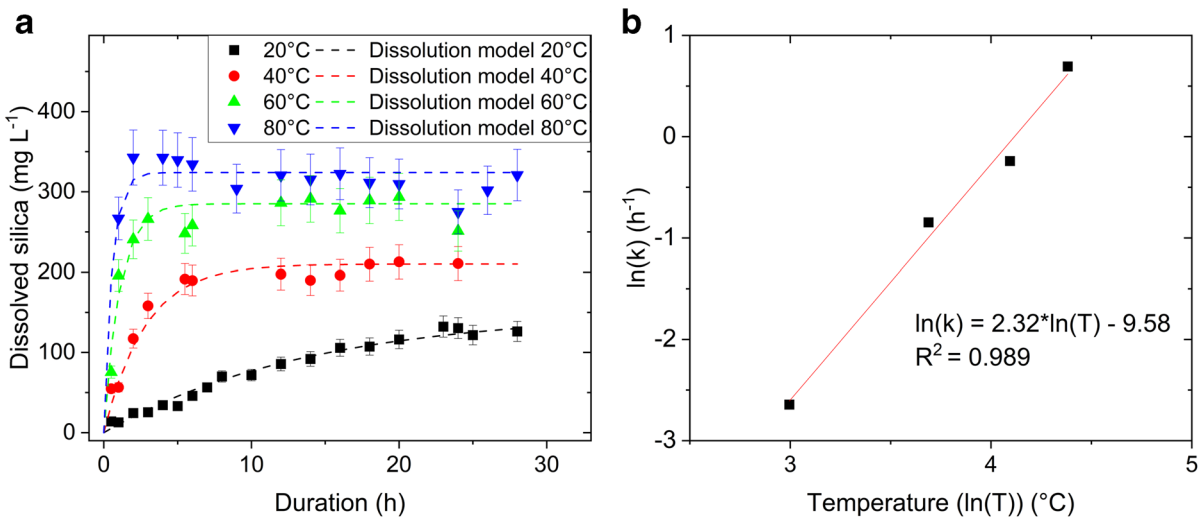

Fig. 2 **a** Theoretical dissolution models deduced from of the data points by applying Eqs. (5), (4), and (2) at the respective temperatures. **b** Correlation of the dissolution constant k and the temperature plotted on a double logarithmic scale

Effect of pH

Apart from the temperature, the pH value of the aqueous solution strongly affects the silica nanoparticle dissolution. Natural waters vary considerably in pH values and range mostly from pH 3 to pH 10 [83–85], which also covers almost the range of pH-values in human bodies [86]. Additionally, it should be pointed out that while tissues exhibit under physiological conditions a fixed pH of 7.4, the pH in the environment of tumors and infectious bacterial often drops to acidic pH ranges [87, 88]. Hence, the relevance of pH value on the dissolution and degradation processes is a pivotal aspect for biomedical applications. Figure 3 shows the dissolved silica concentration in different pH buffer solutions after 24 h (Fig. 3a) and over a time interval of 107 days (Fig. 3b).

Acidic pH

Under acidic conditions, the concentration of the dissolved silica is low after 24 h (Fig. 3a) and increases constantly with time (Fig. 3b). This slow dissolution kinetic can help explain the different saturation concentrations reported in literature for acidic pH conditions [36, 40, 82, 89]. While the lowest silica solubility is expected at neutral pH values [36], Fig. 3a shows that the lowest silica concentration after 24 h is observed under acidic conditions as the dissolution rate is slowed down. Furthermore, the polymerization and depolymerization rate is proportional to the availability of H^+ species at pH values between 3 and 7 [36, 37, 90].

Neutral pH

The pH 6 sample shows the transition from acidic and neutral pH values. The dissolved silica concentration after 24 h in pH 6 buffer solution (Fig. 3a) is lower than at neutral pH after the similar time period, but increasing faster over time than the dissolved silica concentration in acidic pH samples (Fig. 3b). In contrast, neutral to slightly alkaline buffer solutions (pH 7 to pH 9) stay constant over time and show a SSC of about 150 mg L^{-1}. The dissolution is fast and the equilibrium is reached in less than 24 h.

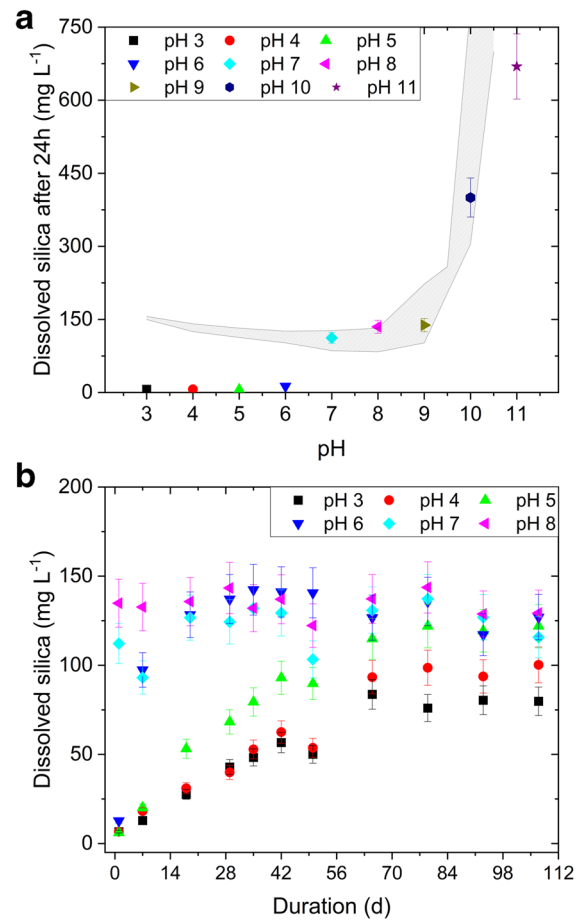

Fig. 3 Impact of pH value on SSC and silica dissolution at room temperature. pH buffer solutions serve to maintain the pH and are not affected by dissolution of silica nanoparticles. **a** Dissolved silica after 24 h. The gray area represents the SSC at the respective pH values and is derived from literature data [36, 37, 40, 82]. After 24 h, the SSC was not reached under acidic conditions. The SSC does not significantly differ between acidic and neutral conditions but show a drastically increase with increasing alkalinity. **b** Equilibrium was not reached with 24 h under acidic conditions, since acidic conditions slow down the dissolution kinetics drastically. The dissolution was therefore monitored over 107 days and is compared to the constant behavior under neutral pH values. The error bars are determined by the deviations of standard solutions to the calibration line

Alkaline pH

Alkaline pH values show the highest dissolved silica concentration after 24 h (Fig. 3a) and a sharp increase of the SSC (gray area in Fig. 3a) in contrast to the acidic and neutral pH value SSC. This can be

explained by the silica species distribution. At acidic and neutral pH levels, the H_4SiO_4 species is the predominant silica species whereas at alkaline pH above pH 9.8, the $H_3SiO_4^-$ becomes predominant and leads to an increase of the silica equilibrium concentration [36]. Furthermore, alkaline pH values catalyze the formation of deprotonated silica species through the availability of OH^- ions and enhance silica solubility [40, 41, 43, 82, 90, 91].

Stability in complex solutions

The salinity of natural waters and biological media can vary considerably [92, 93]. Natural waters can have a broad range of salinity, from freshwater to seawater with about 35 g L^{-1} salt [94, 95]. Geothermal fluids can range up to 150 g L^{-1} salt concentration and in extreme cases to even higher than the Dead Sea's 330 g L^{-1} salt concentration [95, 96]. First, the impact of sodium, potassium, and calcium is studied independently to identify the influence of each cation. Then, the effects were combined by testing the stability of silica nanoparticles in biological relevant media at 37 °C mimicking human body environment.

Ion valence

Figure 4a displays the dissolved silica concentration in NaCl-, KCl-, and $CaCl_2$-solutions over a 24-h time period at room temperature. Low salinities up to 0.5 mol L^{-1} exhibit only a negligible effect on the overall solubility of silica, whereas salinities above 1 mol L^{-1} decrease the solubility drastically (−58% for Na^+, −26% for K^+, −96% for Ca^{2+}). This behavior can be explained with the "salting-out" effect [97]. The impact on the solubility can be ordered as follows $K^+ < Na^+ << Ca^{2+}$ for salt concentrations above 1 mol L^{-1}. The impact of monovalent ions is further ordered by the reverse order of the ionic radii and follows the Hofmeister series [98]. This order can be explained by the hydration number of the cation. An increase of the hydration number leads to a decreasing silica solubility [97, 99]. Highly saline solutions, especially those containing high concentrations of divalent cations, seem to stabilize the silica nanoparticles against dissolution by reducing the water's activity coefficient and consequently lowering the silica solubility. Further studies on ζ-potential evolution at different salinities should be performed.

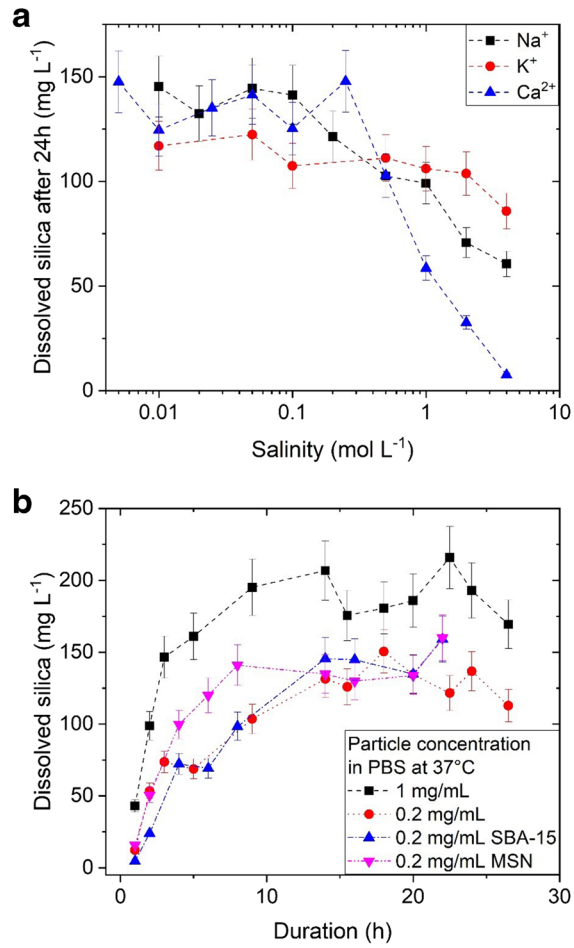

Fig. 4 Dissolution of silica in complex solutions. **a** Dissolved silica in electrolyte solutions at room temperature after 24 h. Higher salinities lower the SSC. Divalent ions have greater effect than monovalent. **b** Evolution of dissolved silica concentration over time in phosphate-buffered saline (PBS) at 37 °C. The nanoparticle concentrations are varied to be comparable with biological applications. Unless otherwise noted, nonporous nanoparticles are used. For details regarding the silica particles used, see Materials and methods. The error bars are determined by the deviations of standard solutions to the calibration line

Literature data indicate the formation of a shielding layer of cations at the diffusive double layer affecting the ζ-potential [98, 100–103], thus affecting the dissolution process.

Physiological buffer

Although the salinity in biological systems is much lower than in natural waters, salinity effects can

still be present when using, e.g., phosphate-buffered saline (PBS, cations Na and K) or simulated body fluids (SBF, cations mainly Na, subordinate K, Ca, and Mg) [73, 92, 104, 105]. Figure 4b shows the dissolution behavior of silica in simplified physiological media using PBS at 37 °C. The nonporous silica nanoparticle concentration was varied to be comparable with the experiments reported in Fig. 1 (1 mg mL^{-1}) and in biological applications (0.2 mg mL^{-1}). Furthermore, the stability of mesoporous silica SBA-15 (< 150 µm, pore size 6 nm, purchased from Sigma-Aldrich, assay 99.9%), and MSN (500 nm, pore size 2 nm, purchased from Sigma-Aldrich, assay 99.9%) was tested as well. The SSC observed in the experiments is about 150–200 mg L^{-1} and corresponds to the toxic silica nanoparticle concentration of above 200 mg L^{-1} identified in literature [55, 56, 60, 106]. If the SSC is reached, further silica nanoparticle dissolution is prevented as long as no silica is removed from the system, e.g., by excretion or digestion. The dose-dependent toxicity of silica nanoparticles may be greatly affected by the availability of silica and the SSC. Solutions having an excess silica concentration (ESC) can be assumed to be more toxic, as the particles cannot be completely dissolved due to the saturation limit of silica in solution. Therefore, for, e.g., design of toxicity studies, detailed knowledge of the SSC of the particles used as well as the dissolution kinetics are crucial factors. The faster dissolution of the MSN (pink downward pointing triangle) in comparison to the nonporous silica nanoparticles of the same concentration (red dot) is in accordance with Lindén and co-workers [104]. They concluded that mesoporous particles are less stable due to large pore volumes, low wall thickness, and crystallization defects in the silica structure. However, although our silica nanoparticles are nonporous and about 3500 times smaller than the SBA-15 particles, the dissolution rate of 0.2 mg mL^{-1} silica nanoparticles (red dot) and SBA-15 (blue triangle) is similar. Surprisingly, the silica nanoparticles with a concentration of 1 mg mL^{-1} (black square) show the highest dissolution rate and the highest dissolved silica concentration, raising the question of the impact of the availability of silica.

Availability of silica

The availability of silica can be either defined as silica dissolved from the nanoparticles or as silica initially present in form of silica in solution. While silica available from particle dissolution is represented in several studies in a simplified form as different particle concentrations or dosages [67, 70, 77, 105, 107], the dissolved silica in solution is disregarded. However, especially for multiple exposure studies in biomedical applications, the dissolved silica concentration should be considered when the time interval is too short for clearance and complete excretion of the silica nanoparticles and their degradation products [72, 108]. Furthermore, silica is ubiquitous in natural waters from weathering of and/or lixiviation from Si-bearing minerals [36]. The availability of silica is an important factor, as the dissolution kinetic is affected by the distance to the saturation level (see Eq. (2)).

Particle concentration/dosage

To order systematically the effects of particle concentration/dosage, three different cases must be distinguished. In case 1, the particle concentration is below the SSC, which means full dissolution of the particles would result in an undersaturated solution (i.e., $c(Si)_{particles} < c(Si)_{SSC}$). In case 2, the particle concentration is equal to the SSC, which means that dissolving all particles would result in an equilibrium solution (i.e., $c(Si)_{particles} \approx c(Si)_{SSC}$). Finally, in case 3, the particle concentration is higher than the SSC, which means that equilibrium between particles and solution occurs with remaining particles (i.e., $c(Si)_{particles} > c(Si)_{SSC}$). All three different cases are shown in Fig. 5a. The gray area represents the SSC. For case 1 (i.e., $c(Si)_{particles} < c(Si)_{SSC}$), particle concentrations of 0.05 mg mL^{-1} and 0.1 mg mL^{-1} are tested (red dot, black square in Fig. 5a). Both experiments show the lowest dissolution rates, as expected due to lowest surface area available for dissolution [16, 77, 109]. The solutions do not reach SSC and consequently are not in equilibrium. For case 2 (i.e., $c(Si)_{particles} \approx c(Si)_{SSC}$), silica nanoparticle concentration of 0.15 mg mL^{-1} (green triangle, Fig. 5a) is used. As expected, the solution reaches the SSC range and leads to an apparent equilibrium state. For case 3 (i.e., $c(Si)_{particles} > c(Si)_{SSC}$), the dissolution behavior of silica nanoparticles is tested at concentrations

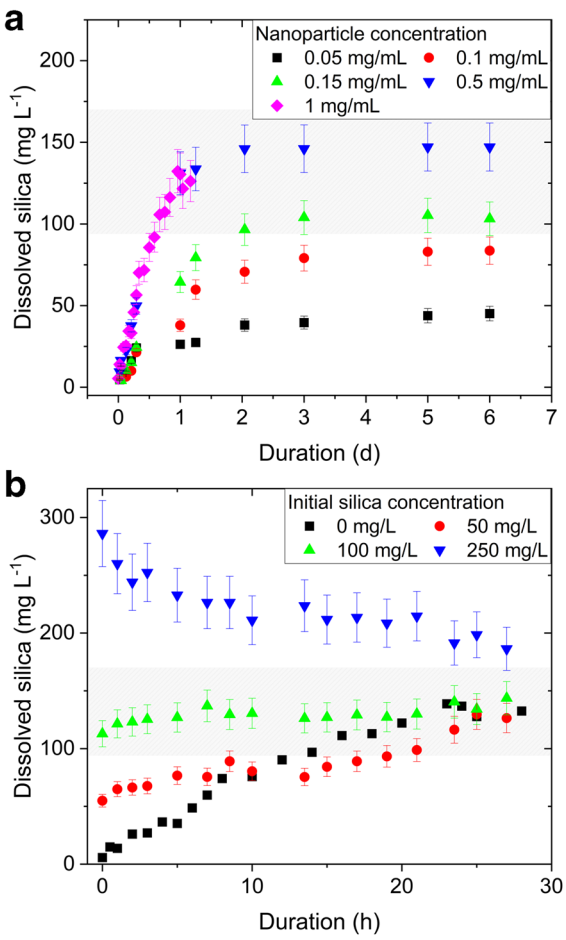

Fig. 5 Effect of silica availability on dissolution of silica nanoparticles in deionized water at room temperature over time. **a** Impact of silica nanoparticle concentration on the dissolution. Gray area represents the SSC. Undersaturated solutions cannot reach the SSC due to limited availability of silica. Dissolution speed depends on the particle concentration. **b** Effect of initial silica concentration in solution. The silica nanoparticle concentration was 1 mg mL^{-1} and consequently oversaturated for all trials. The higher the initial silica concentration in solution, the lower the dissolution speed. In initially oversaturated solutions (250 mg L^{-1}), silica starts precipitating and therefore the concentration decreases over time. The error bars are determined by the deviations of standard solutions to the calibration line

of 0.5 mg mL^{-1} and 1 mg mL^{-1} (pink diamond, blue triangle pointing down, Fig. 5a). Solutions with silica nanoparticles concentrations above the SSC have an ESC and exhibit the highest dissolution rates which is what can be expected due to large surface area available for dissolution [105]. The equilibrium at the SSC is reached within 24 h. Further, 0.5 mg mL^{-1} and 1 mg mL^{-1} show similar behavior, leading to the tentative conclusion that the ESC may not be the driving factor for dissolution rates, but the amount of surface area available for dissolution. In accordance, Rimer et al. [110] and Diedrich et al. [111] found that the dissolution rate neither depends on number density nor directly on particle radius of nanoparticles. The ESC is therefore not expected to affect the dissolution rate but since a higher surface area is available for dissolution, consequently, the SSC is reached faster.

Initial silica concentration

Another important yet overlooked factor for particle stability is the initial silica concentration in solution (Fig. 5b). As expected, the dissolution rate is highest if starting far from equilibrium (0 mg L^{-1}). The higher the initial silica concentration in solution, the slower the dissolution of the particles takes place, which is what can be expected. In supersaturated solutions, the mechanism is reversed. Thus, instead of dissolving the particles, the particles act as nuclei and remove dissolved silica from water. This process seems to be rather slow, since equilibrium was not reached within the period of the experiments. However, data from Fleming [112]indicate the presence of a so-called pseudo-equilibrium point, which is at about 200 mg L^{-1} at room temperature. At this point, the monomeric silica concentration in solution seems to be pseudo-equilibrated and further polymerization and consequently precipitation rate is drastically decreased. Probably, this may explain the resulting high dissolved silica concentration in solution for the experiment with supersaturated solution (blue downward pointing triangle, Fig. 5). In SEM images, formation of new ~ 8 nm size particles as well as regrown particles are visible (Fig. S 2). This phenomenon is known from geothermal systems where high silica concentrations are characteristic and oversaturation is a common technical problem. Silica removal from geothermal fluids using silica particles as seeding material has been identified previously as element-selective and reduces the fouling potential [81, 113, 114]. The formation of silica nanoparticles under geothermal conditions, i.e., in hot, supersaturated solutions, is studied by Tobler and Benning [115] and under in situ conditions by Tamura et al. [116]. They conclude that particle growth is induced by temperature or pH drop during geothermal production. The

finale size of the particles observed was about 5 nm. However, the silica removal displayed in Fig. 4b was induced solely by addition of silica nanoparticles as the similar reference fluid does not exhibit a significant decrease of silica concentration over a 20-day time period; the added silica nanoparticles act therefore unequivocally as nuclei to the aqueous silica.

Surface treatment

Chemical coating

For chemical surface modifications, grafting of (alkoxy)silanes and paraffin as well as a coating with the metal oxide titania were chosen to represent the broad spectrum of modification methods. For paraffin coating, dotriacontan was grafted on the octadecytrimethoxysilane-coated particles; for silanization, two different silanes were used: the dipodal 1,2-Bis(trimethoxysilyl)decane and octadecytrimethoxysilane. Of these chemical surface protection methods, octadecyltrimethoxysilane is the most effective protection layer, leading to a dissolved silica concentration of about 30 mg L^{-1} after 28 days (dotriacontan: 40 mg L^{-1}, titania coating: 47 mg L^{-1}, 1,2-Bis(trimethoxysilyl)decane: 97 mg L^{-1}). In comparison, untreated particles have a saturation concentration of about 150 mg L^{-1}.

Calcination

As expected, calcination of the particles turned out to be the most effective protective procedure (Fig. 6). However, calcination may hinder the synthesis of fluorescent silica nanoparticles, as elevated temperatures can negatively affect the functionality of guest molecules such as organic dyes. Therefore, calcination was performed on non-porous, non-fluorescent silica nanoparticles (Stöber-type) and are compared to the same type of non-calcined particles. The particles in the experiments were calcined at 300 °C, 500 °C, and 700 °C for 24 h. The concentrations after 28 days are 14 mg L^{-1} (calcined 300 °C), 6 mg L^{-1} (calcined 500 °C), and 2 mg L^{-1} (calcined 700 °C) and are below the expected SSC for untreated particles by a factor of 11, 25, and 75, respectively. An explanation for the effective stabilizing behavior of calcination can be given by the FT-IR ATR spectra of calcined and none-calcined silica particles (Fig. 7). The

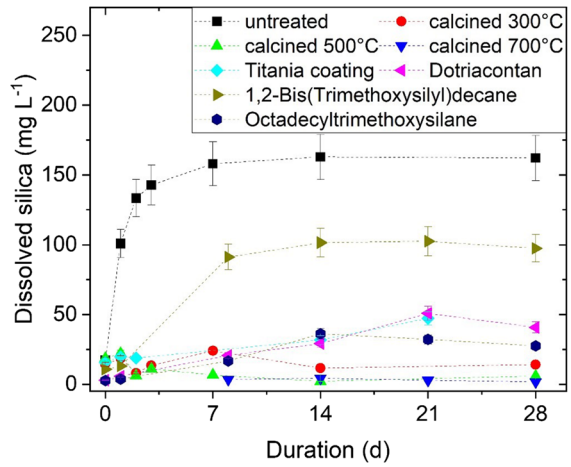

Fig. 6 Stability enhancement treatments and their effect on dissolution of silica nanoparticles (1 mg mL^{-1}) at room temperature. Untreated particles exhibit fast dissolution, whereas the surface modified particles remain more stable over at least 4 weeks. The most effective stabilizing method is calcination at 300 °C, 500 °C, and 700 °C. Coating of the particles with titania, dotriacontane, and octadecyltrimethoxysilane also decreases the silica solubility effectively but not as effective as calcination. 1,2-Bis(trimethoxysilyl)decane shows the lowest impact on the stability of the nanoparticles, but the dissolved silica concentration is still lower than that of untreated nanoparticles after 4 weeks

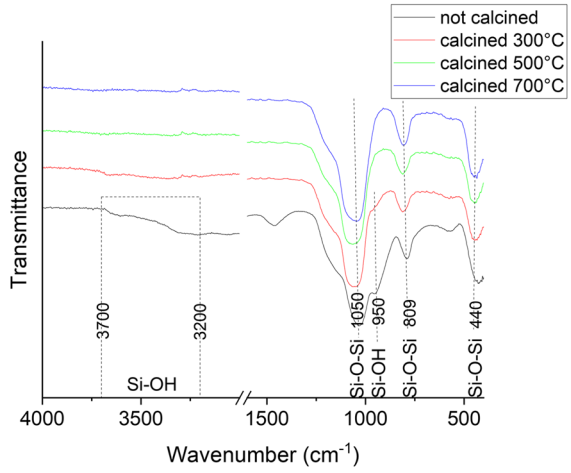

Fig. 7 FT-IR ATR spectra of silica nanoparticles. The untreated particles (not calcined) have both silanol (Si–OH) and siloxane (Si–O-Si) bonds, whereas with increasing calcination temperature, the siloxane bonds become dominant and the silanol bonds disappear

comparison of the non-calcined silica particles and calcined ones at 300 °C, 500 °C, and 700 °C clearly shows the disappearance of Si–OH bonds (band at 950 cm^{-1} and a broad shoulder at 3700–3200 cm^{-1} [117]) with increasing temperatures. The silanol groups on the surface of silica are the point of attack for dissolution of silica nanoparticles [36, 118, 119], and the calcination condensates these silanol groups into more stable siloxane bonds. Rehydroxylation of the surface is expected especially if the silica is exposed to aqueous media [120, 121]. However, the rehydroxylation rate appears to be low as no significant increase of the solubility of the calcined particles was observed over 28 days. In contradiction to previous studies where for effective silanol removal temperatures of at least 500–550 °C are required [122], our data indicate stabilization already from 300 °C.

Conclusion

Many research areas regard silica nanoparticles as stable and inert in a simplistic way, but the stability of silica nanoparticles is in fact highly dependent on the system parameters and the time scale. Especially long-term stability is a crucial characteristic for, e.g., environmental or slow-drug release applications. The main factors affecting the silica saturation concentration (SSC) and dissolution kinetics are temperature, pH-value, and salinity. In addition, other factors may also play a role such as the shape, size, porosity, and morphology of the nanoparticles.

For biomedical applications, the impact of pH on degradation and dissolution kinetic should be carefully examined since the pH in human environment change considerably (e.g., gastric juice, vicinity of tumors). Furthermore, drug release from surface-modified mesoporous silica nanoparticles exhibits areas of plain silica surfaces to the aqueous environment, thus promoting the particle dissolution. Especially for biological applications, the impact of surface modifications, protein corona and ligand instability on the dissolution behavior, the SSC and the residence time could help gaining more control over the biodegradation process of silica nanoparticles in vivo. For some applications like hydrological applications or long-term drug release, improved stability of silica may be desired. Enhancing the stability could be reached by surface modifications or calcination of the particles. Especially calcination increases the stability drastically due to condensation of silanol bonds into more stable siloxane bonds. However, calcinating may not be suitable for all applications (e.g., bioimaging, environmental tracing techniques), especially those where guest molecules are embedded in the nanoparticles during the silica condensation stage of the particle synthesis.

The stability of silica nanoparticles is a major issue for applications in all aqueous environments. Neither the stability nor the degradability of silica nanoparticles should be taken for granted. Instead, silica nanoparticles should be adapted, i.e., via surface treatment such as silanization or calcination where long-term stability is desired or low dosages for lowered risk of toxic side effects. By identifying the parameters in the system reducing the stability or accelerating the dissolution and factors lowering the dissolution rates, the behavior of silica nanoparticles in aqueous environments can be characterized and tuned to fit the specific requirements.

Acknowledgements Thanks to the reviewers and the editors for their constructive suggestions that helped us to improve the manuscript substantially. This study is part of the subtopic "Geoenergy" in the program "MTET—Materials and Technologies for the Energy Transition" of the Helmholtz Association.

Funding Open Access funding enabled and organized by Projekt DEAL.

Data Availability The data that support the findings of this study are available from the authors upon reasonable request.

Declarations

Competing interest The authors declare no competing interests.

References

1. Jeelani PG, Mulay P, Venkat R, Ramalingam C (2019) Multifaceted application of silica nanoparticles. A Review. Silicon 12:1337–1354
2. Scientific Committee on Consumer Safety (SCCS) (2019) OPINION ON solubility of Synthetic Amorphous Silica (SAS), Report Number SCCS/1606/19. European Union, Luxembourg. https://doi.org/10.2875/776214
3. Andersson J, Rosenholm J, Areva S, Lindén M (2004) Influences of material characteristics on ibuprofen drug loading and release profiles from ordered micro- and mesoporous silica matrices. Chem Mater 16:8
4. Liong M, Lu J, Kovochich M, Xia T, Ruehm SG, Nel AE, Tamanoi F, Zink JI (2008) Multifunctional Inorganic Nanoparticles for Imaging, Targeting and Drug Delivery. ACS Nano 2:8
5. Tourne-Peteilh C, Begu S, Lerner DA, Galarneau A, Lafont U, Devoisselle J-M (2011) Sol–gel one-pot synthesis in soft conditions of mesoporous silica materials ready for drug delivery system. J Sol-Gel Sci Technol 61:455–462
6. Kwon S, Singh RK, Perez RA, Abou Neel EA, Kim HW, Chrzanowski W (2013) Silica-based mesoporous nanoparticles for controlled drug delivery. J Tissue Eng 4. https://doi.org/10.1177/2041731413503357
7. van Rijt SH, Bölükbas DA, Argyo C, Datz S, Lindner M, Eickelberg O, Königshoff M, Bein T, Meiners S (2015) Protease-mediated release of chemotherapeutics from mesoporous silica nanoparticles to ex vivo human and mouse lung tumors. ACS Nano 3:13
8. Wang Y, Zhao Q, Han N, Bai L, Li J, Liu J, Che E, Hu L, Zhang Q, Jiang T, Wang S (2015) Mesoporous silica nanoparticles in drug delivery and biomedical applications. Nanomedicine 11:15
9. Bharti C, Nagaich U, Pal AK, Gulati N (2015) Mesoporous silica nanoparticles in target drug delivery system: A review. Int J Pharm Investig 5:10
10. Song Y, Li Y, Xu Q, Liu Z (2017) Mesoporous silica nanoparticles for stimuli-responsive controlled drug delivery: advances, challenges, and outlook. Int J Nanomedicine 12:24
11. Tonelli FMP, Tonelli FCP, Ferreira DRC, da Silva KE, Cordeiro HG, OuchidaV, de Melo Nunes NA (2020) Biocompatibility and functionalization of nanomaterials. Intell Nanomater Drug Deliv Appl. https://doi.org/10.1016/B978-0-12-817830-0.00005-9
12. Maggini L, Cabrera I, Ruiz-Carretero A, Prasetyanto EA, Robinet E, De Cola L (2016) Breakable mesoporous silica nanoparticles for targeted drug delivery. Nanoscale 8:8
13. Bouchoucha M, Côté M-F, Gaudreault RC, Fortin M-A, Kleitz F (2016) Size-controlled functionalized mesoporous silica nanoparticles for tunable drug release and enhanced anti-tumoral activity. Chem Mater 28:16
14. Cheng S-H, Lee C-H, Chen M-C, Souris JS, Tseng F-G, Yang C-S, Mou C-Y, Chen C-T, Lo L-W (2010) Trifunctionalization of mesoporous silica nanoparticles for comprehensive cancer theranostics—the trio of imaging, targeting and therapy. J Mater Chem 20:9
15. Zhao Y-L, Li Z, Kabehie S, Botros YY, Stoddard JF, Zink JI (2010) pH-Operated nanopistons on the surface of mesoporous silica nanoparticles. J Am Chem Soc 132:10
16. Yamada H, Urata C, Aoyama Y, Osada S, Yamauchi Y, Kuroda K (2012) Preparation of colloidal mesoporous silica nanoparticles with different diameters and their unique degradation behavior in static aqueous systems. Chem Mater 24:10
17. Zhao S, Zhang S, Ma J, Fan L, Yin C, Lin G, Li Q (2015) Double loaded self-decomposable SiO(2) nanoparticles for sustained drug release. Nanoscale 7:10
18. Ow H, Larson DR, Srivastava M, Baird BA, Webb WW, Wiesner U (2005) Bright and stable core-shell fluorescent silica nanoparticles.pdf. Nano Lett 5:5
19. Wang F, Tan WB, Zhang Y, Fan X, Wang M (2006) Luminescent nanomaterials for biological labelling. Nanotechnology 17:R1–R13. https://doi.org/10.1088/0957-4484/17/1/R01
20. Gubala V, Giovannini G, Kunc F, Monopoli MP, Moore CJ (2020) Dye-doped silica nanoparticles: synthesis, surface chemistry and bioapplications. Cancer Nanotechnol 11:43
21. Sola F, Canonico B, Montanari M, Volpe A, Barattini C, Pellegrino C, Cesarini E, Guescini M, Battistelli M, Ortolani C, Ventola A, Papa S (2021) Uptake and intracellular trafficking studies of multiple dye-doped core-shell silica nanoparticles in lymphoid and myeloid cells. Nanotechnol Sci Appl 14:29–48
22. Korzeniowska B, Nooney R, Wencel D, McDonagh C (2013) Silica nanoparticles for cell imaging and intracellular sensing. Nanotechnology 24:20
23. Barandeh F, Nguyen PL, Kumar R, Iacobucci GJ, Kuznicki ML, Kosterman A, Bergey EJ, Prasad PN, Gunawardena S (2012) Organically modified silica nanoparticles are biocompatible and can be targeted to neurons in vivo. PLoS One 1(1):e29424
24. Käß W (2004) Geohydrologische Markierungstechnik. Borntraeger, Stuttgart
25. Kasnavia T, Vu D, Sabatini DA (1999) Fluorescent dye and media properties affecting sorption and tracer selection. Groundwater 37:6
26. Magal E, Weisbrod N, Yakirevich A, Yechieli Y (2008) The use of fluorescent dyes as tracers in highly saline groundwater. J Hydrol 358:10
27. Zhu H, Derksen RC, Krause CR, Fox RD, Brazee RD, Ozkan HE (2005) Fluorescent intensity of dye solutions under different pH conditions. J ASTM Int 2:7
28. Paunescu D, Puddu M, Soellner JO, Stoessel PR, Grass RN (2013) Reversible DNA encapsulation in silica to produce ROS-resistant and heat-resistant synthetic DNA "fossils." Nat Protoc 8:9
29. Clemente A, Moreno N, Lobera MP, Balas F, Santamaria J (2016) Fluorescently labelled SiO2 nanoparticles as tracers in natural waters: dependence of detection limits on environmental conditions. Environ Sci Nano 3:7
30. Kong XZ, Deuber CA, Kittila A, Somogyvari M, Mikutis G, Bayer P, Stark WJ, Saar MO (2018) Tomographic reservoir imaging with DNA-labeled silica nanotracers: the first field validation. Environ Sci Technol 52:9

31. Liao R, Yang P, Wu W, Luo D, Yang D (2018) A DNA tracer system for hydrological environment investigations. Environ Sci Technol 52:9
32. Mikutis G, Deuber CA, Schmid L, Kittila A, Lobsiger N, Puddu M, Asgeirsson DO, Grass RN, Saar MO, Stark WJ (2018) Silica-encapsulated DNA-based tracers for aquifer characterization. Environ Sci Technol 52:11
33. Alaskar M, Ames M, Liu C, Li K, Horne R (2015) Temperature nanotracers for fractured reservoirs characterization. J Petrol Sci Eng 127:17
34. Zhang YM, T. S, Li K, Horne RN (2016) Uniquely identifiable DNA-embedded silica nanotracer for fractured reservoir characterization. In: 41st Workshop on geothermal reservoir engineering. Stanford University, Stanford, CA, p 10
35. Rudolph B, Berson J, Held S, Nitschke F, Wenzel F, Kohl T, Schimmel T (2020) Development of thermo-reporting nanoparticles for accurate sensing of geothermal reservoir conditions. Sci Rep 10:11422
36. Iler RK (1979) The chemistry of silica. Solubility, polymerization, colloid and surface properties, and biochemistry. John Wiley & Sons, Chichester, p 866
37. Okamoto G, Okura T, Goto K (1957) Properties of silica in water. Geochim Cosmochim Acta 12:10
38. Gunnarsson I, Arnórsson S (2000) Amorphous silica solubility and the thermodynamic properties of H4SiO°4 in the range of 0° to 350°C at Psat. Geochim Cosmochim Acta 64:13
39. Fournier RO, Rowe JJ (1966) Estimation of underground temperature. AJS 264:13
40. Alexander GB, Heston WM, Iler RK (1954) The solubility of amorphous silica in water. J Phys Chem 58:3
41. Greenberg SA, Price EW (1957) The solubilty of silica in solutions of electrolytes. J Phys Chem 61:3
42. Rimstidt JD, Barnes HL (1980) Kinetics of silica water reactions. Geochim Cosmochim Acta 44:17
43. Eikenberg J (1990) On the problem of silica solubility at high pH. Paul Scherrer Institut, Villigen, Switzerland
44. Nitschke F, Held S, Villalon I, Neumann T, Kohl T (2017) Assessment of performance and parameter sensitivity of multicomponent geothermometry applied to a medium enthalpy geothermal system. Geotherm Energy 5:12. https://doi.org/10.1186/s40517-017-0070-3
45. Morey GW, Fournier RO, Rowe JJ (1962) The solubility of quartz in water in the temperature interval from 25° to 300°C. Geochim Cosmochim Acta 26:16
46. Arnórsson S (1975) Application of the silica geothermometer in low temperature hydrothermal areas in iceland. Am J Sci 275:22
47. Yamamoto E, Kuroda K (2016) Colloidal mesoporous silica nanoparticles. Bull Chem Soc Jpn 89:501–539
48. Lin W, Huang YW, Zhou XD, Ma Y (2006) In vitro toxicity of silica nanoparticles in human lung cancer cells. Toxicol Appl Pharmacol 217:8
49. Chang J-S, Ke Liang B, Hwang D-F, Kong Z-L (2007) In vitro cytotoxicity of silica nanoparticles at high concentrations strongly depends on the metabolic activity type of the cell line. Environ Sci Technol 41:5
50. Corbalan JJ, Medina C, Jacoby A, Malinski T, Radomski MW (2011) Amorphous silica nanoparticles trigger nitric oxide/peroxynitrite imbalance in human endothelial cells: inflammatory and cytotoxic effects. Int J Nanomedicine 6:15
51. Park MVDZ, Lynch I, Ramírez-García S, Dawson KA, de la Fonteyne L, Gremmer E, Slob W, Briedé JJ, Elsaesser A, Howard CV, van Loveren H, de Jong WH (2011) In vitro evaluation of cytotoxic and inflammatory properties of silica nanoparticles of different sizes in murine RAW 264.7 macrophages. J Nanoparticle Res 13:13
52. Corbalan JJ, Medina C, Jacoby A, Malinski T, Radomski MW (2012) Amorphous silica nanoparticles aggregate human platelets: potential implications for vascular homeostasis. Int J Nanomedicine 7:9
53. Jiang L, Yu Y, Li Y, Yu Y, Duan J, Zou Y, Li Q, Sun Z (2016) Oxidative damage and energy metabolism disorder contribute to the hemolytic effect of amorphous silica nanoparticles. Nanoscale Res Lett 11:57
54. Bakshi MS (2017) Nanotoxicity in Systemic Circulation and Wound Healing. Chem Res Toxicol 30:20
55. Chen L, Liu J, Zhang Y, Zhang G, Kang Y, Chen A, Feng X, Shao L (2018) The toxicity of silica nanoparticles to the immune system. Nanomedicine 13:24
56. Kersting M, Olejnik M, Rosenkranz N, Loza K, Breisch M, Rostek A, Westphal G, Bunger J, Ziegler N, Ludwig A, Koller M, Sengstock C, Epple M (2020) Subtoxic cell responses to silica particles with different size and shape. Sci Rep 10:21591. https://doi.org/10.1038/s41598-020-78550-5
57. Ye Y, Liu J, Chen M, Sun L, Lan M (2010) In vitro toxicity of silica nanoparticles in myocardial cells. Environ Toxicol Pharmacol 29:7
58. Bhavsar D, Patel V, Sawant K (2019) Systematic investigation of in vitro and in vivo safety, toxicity and degradation of mesoporous silica nanoparticles synthesized using commercial sodium silicate. Microporous Mesoporous Mater 284:343–352
59. Mohammadpour R, Cheney DL, Grunberger JW, Yazdimamaghani M, Jedrzkiewicz J, Isaacson KJ, Dobrovolskaia MA, Ghandehari H (2020) One-year chronic toxicity evaluation of single dose intravenously administered silica nanoparticles in mice and their Ex vivo human hemocompatibility. J Control Release 324:471–481. https://doi.org/10.1016/j.jconrel.2020.05.027
60. Mohammadpour R, Yazdimamaghani M, Cheney DL, Jedrzkiewicz J, Ghandehari H (2019) Subchronic toxicity of silica nanoparticles as a function of size and porosity. J Control Release 304:17
61. Koch J, Doswald S, Mikutis G, Stark WJ, Grass RN (2021) Ecotoxicological Assessment of DNA-tagged silica particles for environmental tracing. Environ Sci Technol 55:9
62. Ale A, Gutierrez MF, Rossi AS, Bacchetta C, Desimone MF, Cazenave J (2021) Ecotoxicity of silica nanoparticles in aquatic organisms: an updated review. Environ Toxicol Pharmacol 87:18
63. Cedervall T, Lynch I, Lindman S, Berggård T, Thulin E, Nilsson H, Dawson KA, Linse S (2007) Understanding the nanoparticle–protein corona using methods to

quantify exchange rates and affinities of proteins for nanoparticles. PNAS 104:6
64. Cauda V, Schlossbauer A, Bein T (2010) Bio-degradation study of colloidal mesoporous silica nanoparticles: effect of surface functionalization with organo-silanes and poly(ethylene glycol). Microporous Mesoporous Mater 132:12
65. Huang X, Teng X, Chen D, Tang F, He J (2010) The effect of the shape of mesoporous silica nanoparticles on cellular uptake and cell function. Biomaterials 31:11
66. Croissant JG, Butler KS, Zink JI, Brinker CJ (2020) Synthetic amorphous silica nanoparticles: toxicity, biomedical and environmental implications. Nat Rev Mater 5:886–909
67. Liberman A, Mendez N, Trogler WC, Kummel AC (2014) Synthesis and surface functionalization of silica nanoparticles for nanomedicine. Surf Sci Rep 69:27
68. Lin YS, Hurley KR, Haynes CL (2012) Critical considerations in the biomedical use of mesoporous silica nanoparticles. J Phys Chem Lett 3:11
69. Quignard S, Coradin T, Powell JJ, Jugdaohsingh R (2017) Silica nanoparticles as sources of silicic acid favoring wound healing in vitro. Colloids Surf B Biointerfaces 155:8
70. Croissant JG, Brinker CJ (2018) Biodegradable silica-based nanoparticles: dissolution kinetics and selective bond cleavage. Enzymes 43:34
71. Linden M (2018) Biodistribution and excretion of intravenously injected mesoporous silica nanoparticles: implications for drug delivery efficiency and safety. Enzymes 43:26
72. He X, Nie H, Wang K, Tan W, Wu X, Zhang P (2008) In vivo study of biodistribution and urinary excretion of surface-modified silica nanoparticles. Anal Chem 80:7
73. Lin YS, Abadeer N, Haynes CL (2011) Stability of small mesoporous silica nanoparticles in biological media. Chem Commun (Camb) 47:3
74. Mahon E, Hristov DR, Dawson KA (2012) Stabilising fluorescent silica nanoparticles against dissolution effects for biological studies. Chem Commun (Camb) 48:3
75. Möller K, Bein T (2019) Degradable drug carriers: vanishing mesoporous silica nanoparticles. Chem Mater 31:15
76. Paris JL, Colilla M, Izquierdo-Barba I, Manzano M, Vallet-Regí M (2017) Tuning mesoporous silica dissolution in physiological environments: a review. J Mater Sci 52:11
77. Croissant JG, Fatieiev Y, Khashab NM (2017) Degradability and clearance of silicon, organosilica, silsesquioxane, silica mixed oxide, and mesoporous silica nanoparticles. Adv Mater 29:1604634. https://doi.org/10.1002/adma.201604634
78. Stöber W, Fink A, Bohn E (1968) Controlled growth of monodisperse silica spheres in the micron size range. J Colloid Interface Sci 26:8
79. Arkles B, Pan Y, Larson GL, Singh M (2014) Enhanced hydrolytic stability of siliceous surfaces modified with pendant dipodal silanes. Chemistry 20:9
80. Joo JB, Zhang Q, Lee I, Dahl M, Zaera F, Yin Y (2012) Mesoporous anatase titania hollow nanostructures though silica-protected calcination. Adv Func Mater 22:9
81. Spitzmüller L, Goldberg V, Held S, Grimmer JC, Winter D, Genovese M, Koschikowski J, Kohl T (2021) Selective silica removal in geothermal fluids: implications for applications for geothermal power plant operation and mineral extraction. Geothermics 95:102141. https://doi.org/10.1016/j.geothermics.2021.102141
82. Krauskopf KB (1956) Dissolution and precipitation of silica at low temperatures. Geochim Cosmochim Acta 10:26
83. Hájek M, Jiménez-Alfaro B, Hájek O, Brancaleoni L, Cantonati M, Carbognani M, Dedić A, Dítě D, Gerdol R, Hájková P, Horsáková V, Jansen F, Kamberović J, Kapfer J, Kolari THM, Lamentowicz M, Lazarević P, Mašić E, Moeslund JE, Pérez-Haase A, Peterka T, Petraglia A, Pladevall-Izard E, Plesková Z, Segadelli S, Semeniuk Y, Singh P, Šímová A, Šmerdová E, Tahvanainen T, Tomaselli M, Vystavna Y, Biţă-Nicolae C, Horsák M (2021) A European map of groundwater pH and calcium. Earth Syst Sci Data 13:1089–1105
84. Gunnarsson I, Arnórsson S (2003) Silica scaling: the main obstacle in efficient use of high-temperature geothermal fluids. In: International Geothermal Conference. World Geothermal Congress, Reykjavík
85. Suzuki Y, Ioka S, Muraoka H (2017) Geothermal Resource Exploration by Stream pH Mapping in Mutsu Hiuchi Dake Volcano, Japan. Energies 10:1009. https://doi.org/10.3390/en10071009
86. Proksch E (2018) pH in nature, humans and skin. J Dermatol 45:9
87. Tannock IF, Rotin D (1989) Acid pH in tumors and its potential for therapeutic exploitation. Cancer Res 49:4373–4384
88. Mura S, Nicolas J, Couvreur P (2013) Stimuli-responsive nanocarriers for drug delivery. Nat Mater 12:13
89. Vogelsberger W, Seidel A, Rudakoff G (1992) Solubility of Silica Gel in Water. J Chem Soc Faraday Trans 88:4
90. Goto K (1956) Effect of pH on polymerization of silicic acid. J Phys Chem 60:2
91. Dove PM, Han N, Wallace AF, De Yoreo JJ (2008) Kinetics of amorphous silica dissolution and the paradox of the silica polymorphs. PNAS 105:6
92. Khlebovich VV (2015) Applied aspects of the concept of critical salinity. Biol Bull Rev 5:562–567
93. Halperin ML, Kamel KS, Goldstein MB (2010) Fluid. Elsevier, Electrolyte & Acid-Base Physiology
94. Durack PJ, Wijffels SE, Boyer TP (2013) Long-term salinity changes and implications for the global water cycle. In: Ocean Circulation and Climate - A 21st Century Perspective. Elsevier, Oxford, UK, pp 727–757. https://doi.org/10.1016/B978-0-12-391851-2.00028-3
95. Neupane G, Wendt DS (2017) Assessment of mineral resources in geothermal brines in the US. In: 42nd Workshop on Geothermal Reservoir Engineering. Stanford University, Stanford, CA
96. Finster M, Clark C, Schroeder J, Martino L (2015) Geothermal produced fluids: characteristics, treatment technologies, and management options. Renew Sustain Energy Rev 50:15
97. Marshall WL, Warakomski JM (1980) Amorphous silica solubilites – II. Effect of aqueous salt solutions at 25°C. Geochim Cosmochim Acta 44:9

98. Parsons DF, Bostrom M, Maceina TJ, Salis A, Ninham BW (2010) Why direct or reversed Hofmeister series? Interplay of hydration, non-electrostatic potentials, and ion size. Langmuir 26:6
99. Stokes RH, Robinson RA (1948) Ionic hydration and activity in electrolyte solutions. J Am Chem Soc 70:9
100. Pianegonda S, Barbosa MC, Levin Y (2005) Charge reversal of colloidal particles. Europhys Lett 71(5). https://doi.org/10.1209/epl/i2005-10150-y
101. Tikhonov A (2006) Compact Layer of Alkali Ions at the Surface of Colloidal Silica. J Phys Chem C 111:8
102. Franks GV (2002) Zeta potentials and yield stresses of silica suspensions in concentrated monovalent electrolytes: isoelectric point shift and additional attraction. J Colloid Interface Sci 249:8
103. Franks GV, Johnson SB, Scales PJ, Boger DV, Healy TW (1999) Ion-specific strenght of attractive particle networks. Langmuir 15:10
104. Braun K, Pochert A, Beck M, Fiedler R, Gruber J, Lindén M (2016) Dissolution kinetics of mesoporous silica nanoparticles in different simulated body fluids. J Sol-Gel Sci Technol 79:9
105. He Q, Shi J, Zhu M, Chen Y, Chen F (2010) The three-stage in vitro degradation behavior of mesoporous silica in simulated body fluid. Microporous Mesoporous Mater 131:7
106. Sun L, Sogo Y, Wang X, Ito A (2021) Biosafety of mesoporous silica nanoparticles: a combined experimental and literature study. J Mater Sci Mater Med 32:102
107. Murugadoss S, Lison D, Godderis L, Van Den Brule S, Mast J, Brassinne F, Sebaihi N, Hoet PH (2017) Toxicology of silica nanoparticles: an update. Arch Toxicol 91:2967–3010
108. Liu T, Li L, Teng X, Huang X, Liu H, Chen D, Ren J, He J, Tang F (2011) Single and repeated dose toxicity of mesoporous hollow silica nanoparticles in intravenously exposed mice. Biomaterials 32:12
109. Kumar D, SailajaChirravuri SV, Shastri NR (2014) Impact of surface area of silica particles on dissolution rate and oral bioavailability of poorly water soluble drugs: a case study with aceclofenac. Int J Pharm 461:10
110. Rimer JD, Trofymluk O, Navrotsky A, Lobo RF, Vlachos DG (2007) Kinetic and thermodynamic studies of silica nanoparticle dissolution. Chem Mater 19:9
111. Diedrich T, Dybowska A, Schott J, Valsami-Jones E, Oelkers EH (2012) The dissolution rates of SiO2 nanoparticles as a function of particle size. Environ Sci Technol 46:7
112. Fleming BA (1986) Kinetics of reaction between silicic acid and amorphous silica surfaces in NaCI solutions. J Colloid Interface Sci 110:40–64. https://doi.org/10.1016/0021-9797(86)90351-6
113. Sugita H, Matsunaga I, Yamaguchi T, Kato K, Ueda A (2003) Silica removal performance of seed from geothermal fluids. Geothermics 32:15
114. Setiawan FA, Rahayuningsih E, Petrus HTBM, Nurpratama MI, Perdana I (2019) Kinetics of silica precipitation in geothermal brine with seeds addition: minimizing silica scaling in a cold re-injection system. Geothermal Energy 7:16
115. Tobler DJ, Benning LG (2013) In situ and time resolved nucleation and growth of silica nanoparticles forming under simulated geothermal conditions. Geochim Cosmochim Acta 114:13
116. Tamura R, Inoue H, Hanajima E, Ikeda R, Osaka Y, Yanaze T, Kusakabe M, Yonezu K, Yokoyama T, Tsukamoto K, Marumo K, Ueda A (2019) In situ observations of silica nanoparticle growth in geothermal brine at the Sumikawa geothermal station, Japan, by dynamic light scattering. Geothermics 77:304–312
117. Socrates G (2004) Infrared and Raman characteristic group frequencies: tables and charts. John Wiley & Sons, Chichester
118. Stöber W (1967) Formation of silicic acid in aqueous suspensions of different silica modifications. In: Equilibrium Concepts in Natural Water Systems. American Chemical Society, New York, NY, pp 161–182. https://doi.org/10.1021/ba-1967-0067.ch007
119. Cypryk M, Apeloig Y (2002) Mechanism of the acid-catalyzed Si-O bond cleavage in siloxanes and siloxanols. Theor Stud Organometallics 21:11
120. Zhuravlev LT (2000) The surface chemistry of amorphous silica. Colloids Surf A Physicochem Eng Asp 173:1–38. https://doi.org/10.1016/S0927-7757(00)00556-2
121. Warring SL, Beattie DA, McQuillan AJ (2016) Surficial siloxane-to-silanol interconversion during room-temperature hydration/dehydration of amorphous silica films observed by ATR-IR and TIR-Raman spectroscopy. Langmuir 32:9
122. Yan F, Jiang J, Chen X, Tian S, Li K (2014) Synthesis and characterization of silica nanoparticles preparing by low-temperature vapor-phase hydrolysis of SiCl4. Ind Eng Chem Res 53:7